A lytic transglycosylase connects bacterial focal adhesion complexes to the peptidoglycan cell wall

Carlos A. Ramírez Carbó[1, 2, 3], Olalekan G. Faromiki[1, 3] and Beiyan Nan[1]*

[1] Department of Biology, Texas A&M University, College Station, TX 77843, USA

[2] The Genetics and Genomics Interdisciplinary Program, Texas A&M University, College Station, TX 77843, USA

[3] C. A. R. C. and O. G. F. contribute equally to this work

*Corresponding author: Beiyan Nan, 306C BSBE, 3258 TAMU, College Station, TX77843

Tel.: 979-845-3487, email: bnan@tamu.edu

Abstract

The Gram-negative bacterium *Myxococcus xanthus* glides on solid surfaces. Dynamic bacterial focal adhesion complexes (bFACs) convert proton motive force from the inner membrane into mechanical propulsion on the cell surface. It is unclear how the mechanical force transmits across the rigid peptidoglycan (PG) cell wall. Here we show that AgmT, a highly abundant lytic PG transglycosylase homologous to *Escherichia coli* MltG, couples bFACs to PG. Coprecipitation assay and single-particle microscopy reveal that the gliding motors fail to connect to PG and thus are unable to assemble into bFACs in the absence of an active AgmT. Heterologous expression of *E. coli* MltG restores the connection between PG and bFACs and thus rescues gliding motility in the *M. xanthus* cells that lack AgmT. Our results indicate that bFACs anchor to AgmT-modified PG to transmit mechanical force across the PG cell wall.

Introduction

In natural ecosystems, the majority of bacteria attach to surfaces[1]. Surface-associated motility is critical for many bacteria to navigate and populate their environments[2]. The Gram-negative bacterium *Myxococcus xanthus* moves on solid surfaces using two independent mechanisms: social (S-) motility and adventurous (A-) motility. S-motility, analogous to the twitching motility in *Pseudomonas* and *Neisseria*, is powered by the extension and retraction of type IV pili[3,4]. A-motility is a form of gliding motility that does not depend on conventional motility-related cell surface appendages, such as flagella or pili[2,5]. AglR, AglQ, and AglS form a membrane channel that functions as the gliding motor by harvesting proton motive force[6,7]. Motor units associate with at least fourteen gliding-related proteins that reside in the cytoplasm, inner membrane, periplasm, and outer membrane[8,9].

In each gliding cell, two distinct populations of gliding complexes coexist: dynamic complexes move along helical paths and static complexes remain fixed relative to the substrate[10-13]. Motors transport incomplete gliding complexes along helical tracks but form complete, force-generating complexes at the ventral side of cells that appear fixed to the substrate (**Fig. 1**)[10,13]. Based on their functional analogy with eukaryotic focal adhesion sites, these complete gliding machineries are called bacterial focal adhesion complexes (bFACs). Despite their static appearance, bFACs are dynamic under single-molecule microscopy. Individual motors frequently display move-stall-move patterns, in which they move rapidly along helical trajectories, join a bFAC where they remain stationary briefly, then move rapidly again toward the next bFAC or reverse their moving directions[11,14,15]. bFACs adhere to the gliding substrate through an outer membrane adhesin[12]. As motors transport bFACs toward lagging cell poles, cells move forward but bFACs remain static relative to the gliding substrate.

48 bFAC assembly can be quantified at nanometer resolution using the single-particle
49 dynamics of gliding motors[11,16]. Single particles of a fully functional, photoactivatable
50 mCherry (PAmCherry)-labeled AglR display three dynamic patterns, stationary,
51 directed motion, and diffusion[11,16]. The stationary population consists of the motors in
52 fully assembled bFACs, which do not move before photobleach. In contrast, the motors
53 moving in a directed manner carry incomplete gliding complexes along helical tracks,
54 whereas the diffusing motors assemble to even less completeness[10,11,13,16]. As motors only
55 generate force in static bFACs[10], the population of nonmotile motors indicates the
56 overall status of fully assembled bFACs.

57 However, how bFACs transmit force across the peptidoglycan (PG) cell wall is
58 unclear. PG is a mesh-like single molecule of crosslinked glycan strands that surrounds
59 the entire cytoplasmic membrane. The rigidity of PG defines cell shape and protects
60 cells from osmotic lysis[17,18]. If bFACs physically penetrate PG, their transportation
61 toward lagging cell poles would tear PG and trigger cell lysis. To avoid breaching PG,
62 an updated model proposes that rather than forming stable and rigid complexes,
63 gliding-related proteins only assemble into force-generating machineries in bFACs.
64 Outside of bFACs, these proteins could localize diffusively or move along with
65 unengaged motor units[10,19]. To simplify this model, we can artificially divide each
66 gliding machinery into two subcomplexes, one on each side of the PG layer. The inner
67 subcomplexes move freely and only assembly with the outer subcomplexes in bFACs,
68 which transform proton motive force into mechanical propulsion on cell surfaces (**Fig.
69 1**).

70 The inner subcomplexes, containing the motors, are the force-generating units in
71 bFACs. As motors reside in the fluid inner membrane, to transmit force to the cell
72 surface, the inner subcomplexes must push against two relatively rigid structures, one

73 on each side of the membrane, in opposite directions[19] (**Fig. 1**). MreB is a bacterial actin
74 homolog that supports rod shape in many bacteria[16,17,20]. In *M. xanthus*, MreB also
75 connects to bFACs on the cytoplasmic side and thus plays essential roles in
76 gliding[2,5,6,12,16,21,22]. The inner subcomplexes could push against MreB filaments and PG in
77 the cytoplasm and periplasm, respectively[10,16,19,23]. The interaction between the inner
78 subcomplexes and PG not only satisfies the physical requirement for force generation
79 but also supports bFAC stability. Without this interaction, the inner and outer
80 subcomplexes can only form transient, "slippery" association, which is predicted to
81 produce short and aberrant cell movements[19]. How the inner complex interacts with PG
82 remains unknown. It was speculated that gliding motors in the inner complex could
83 bind PG directly[10]. However, such binding has not been confirmed by experiments.

84 In this study, we found that AgmT, a lytic transglycosylase (LTG) for PG, is
85 required for *M. xanthus* gliding motility. Whereas AgmT only regulates cell morphology
86 moderately during vegetative growth, it is essential for maintaining PG integrity under
87 the stress from the antibiotic mecillinam. Using single-particle tracking microscopy and
88 coprecipitation assays, we found that AgmT is essential for the inner subcomplexes to
89 connect to PG and stall in bFACs. Importantly, expressing *Escherichia coli* MltG
90 heterologously rescues the connection between PG and bFACs and thus restores gliding
91 motility. Hence, the LTG activity of AgmT anchors bFACs to PG, potentially by
92 modifying PG structure. Our findings reveal the long-sought connection between PG
93 and bFACs that allows mechanical force to transmit across the PG cell wall.

Results

AgmT, a putative LTG, is required for gliding motility.

To elucidate how bFACs interact with PG, we searched for potential PG-binding domains among the proteins that are required for gliding motility. A previous report identified 35 gliding-related genes in *M. xanthus* through transposon-mediated random mutagenesis[24]. Among these genes, *agmT* (ORF K1515_04910[25]) was predicted to encode an inner membrane protein with a single transmembrane helix (residues 4 – 25) followed by a large "periplasmic solute-binding" domain[24]. No other motility-related genes are found in the vicinity of *agmT*. After careful analysis, we found that AgmT showed significant similarity to the widely conserved YceG/MltG family LTGs. The putative active site, Glu223 (corresponding to E218 in *E. coli* MltG)[26], is conserved in AgmT (**Fig. 2A**).

To confirm the function of AgmT in gliding, we constructed an *agmT* in-frame deletion mutant. We further knocked out the *pilA* gene that encodes pilin for type IV pilus to eliminate S-motility. On a 1.5% agar surface, the *pilA*$^-$ cells moved away from colony edges both as individuals and in "flare-like" cell groups, indicating that they were still motile with gliding motility. In contrast, the *ΔaglR pilA*$^-$ cells that lack an essential component in the gliding motor were unable to move outward from the colony edge and thus formed sharp colony edges. Similarly, the *ΔagmT pilA*$^-$ cells also formed sharp colony edges, indicating that they could not move efficiently with gliding (**Fig. 2B**).

We then imaged individual *ΔagmT pilA*$^-$ cells on 1.5% agar surface at 10-s intervals using bright-field microscopy. To our surprise, instead of being static, individual *ΔagmT pilA*$^-$ cells displayed slow movements, with frequent pauses and reversals (**Video 1**). To quantify the effects of AgmT, we measured the velocity and gliding persistency (the

119 distances cells traveled before pauses and reversals) of individual cells. Compared to
120 the *pilA*$^{-}$ cells that moved at 2.30 ± 1.33 μm/min (n = 46) and high persistency (**Video 2**
121 and **Fig. 2C, D**), *ΔagmT pilA*$^{-}$ cells moved significantly slower (0.88 ± 0.62 μm/min, n =
122 59) and less persistent (**Video 1** and **Figure. 2C, D**). Such aberrant gliding motility is
123 distinct from the "hyper reversal" phenotype due to the polarity regulators
124 constitutively switching the moving direction of cells, because hyper reversing cells
125 usually maintain gliding velocity at the wild-type level[27]. Instead, such phenotypes
126 match the prediction that when the inner complexes of bFACs lose connection with PG,
127 bFACs can only generate short, and inefficient movements[19]. Our data indicate that
128 AgmT is not essential component in the bFACs. Thus, AgmT is likely to regulate the
129 assembly and stability of bFACs, especially their connection with PG.

130 **AgmT is an LTG**

131 As AgmT is a putative LTG for PG, we then tested if its predicted active site, Glu223, is
132 required for gliding. Because the amino acid following Glu223 is also a glutamate
133 (Glu224), we replaced both glutamate residues with alanine (AgmT^{EAEA}) using site-
134 directed mutagenesis to alter their codons on the chromosome. *agmT*^{EAEA} *pilA*$^{-}$ cells
135 formed sharp colony edges on agar surface (**Fig. 2B**). Thus, the putative LTG activity of
136 AgmT is required for *M. xanthus* gliding motility.

137 To determine if AgmT is an LTG, we expressed the periplasmic domain (amino
138 acids 25 – 339) of wild-type AgmT and AgmT^{EAEA} in *E. coli*. We purified PG from wild-
139 type *M. xanthus* cells, labeled it with Remazol brilliant blue (RBB), and tested if the
140 purified AgmT variants hydrolyze labeled PG *in vitro* and release the dye[28,29]. Similar to
141 lysozyme that specifically cleaves the β-1,4-glycosidic bonds in PG, wild-type AgmT
142 solubilized dye-labeled *M. xanthus* PG that absorbed light at 595 nm. In contrast, the

143 AgmT^{EAEA} variant failed to release the dye (**Fig. 3A**). Hence, AgmT displays LTG
144 activity *in vitro*.

145 Whereas AgmT does not affect growth rate (**Fig. S2**), cells that lacked AgmT or
146 expressed AgmT^{EAEA} maintained rod shape but were slightly shorter and wider than the
147 wild-type ones (**Fig. 3B**). Nevertheless, altered morphology alone does not likely
148 account for abolished gliding. In fact, a previously reported mutant that lacks all three
149 class A penicillin-binding proteins (*Δ3*) displays similarly shortened and widened
150 morphology[30] but is still motile by gliding (**Fig. S1**).

151 A recent report revealed that *Vibrio cholerae* MltG degrades un-crosslinked PG
152 turnover products and prevents their detrimental accumulation in the periplasm[31]. To
153 test if AgmT plays a similar role in *M. xanthus*, we used mecillinam to induce cell
154 envelope stress. Mecillinam is a β-lactam that induces the production of toxic, un-
155 crosslinked PG strands[32]. Rather than collapsing the rod shape, mecillinam only causes
156 bulging near the centers of wild-type *M. xanthus* cells, whereas large-scale cell lysis does
157 not occur, and cell poles still maintain rod shape even after prolonged (20 h) treatment
158 (**Fig. 3C**)[30]. Thus, wild-type *M. xanthus* can largely mitigate mecillinam stress. In
159 contrast, mecillinam-treated *agmT* cells increased their width drastically, displayed
160 significant cell surface irregularity along their entire cell bodies, and lysed frequently
161 (**Fig. 3C**). Cells expressing AgmT^{EAEA} as the sole source of AgmT displayed similar, but
162 even stronger phenotypes under mecillinam stress, growing into elongated, twisted
163 filaments that formed multiple cell poles and lysed frequently (**Fig. 3C**). These results
164 confirm that similar to *V. cholerae* MltG, *M. xanthus* AgmT is important for maintaining
165 cell integrity under mecillinam stress. The different responses from *agmT* and *agmT^{EAEA}*
166 cells suggest that other LTGs could partially substitute AgmT while AgmT^{EAEA} blocks
167 these enzymes from accessing un-crosslinked PG strands.

168 AgmT is the only LTG *in M. xanthus* that belongs to the YceG/MltG family. Besides
169 *agmT*, the genome of *M. xanthus* contains 13 genes that encode putative LTGs (**Table**
170 **S1**). To test if these proteins also contribute to gliding, we knocked out each of these 13
171 genes in the *pilA*$^{-}$ background. The resulting mutants all retained gliding motility,
172 indicating that AgmT is the only LTG that is required for *M. xanthus* gliding (**Fig. S1**).

173 **AgmT is essential for proper bFACs assembly**

174 How does AgmT support gliding? We first tested if AgmT regulates the function of the
175 gliding motor. For this purpose, we quantified the motor dynamics by tracking single
176 particles of AglR, an essential component of the motor. We spotted the cells that express
177 a fully functional, photo-activatable mCherry (PAmCherry)-labeled AglR[11] on 1.5% agar
178 surface. We used a 405-nm excitation laser to activate the fluorescence of a few labeled
179 AglR particles randomly in each cell and quantified their localization using a 561-nm
180 laser at 10 Hz using single particle tracking photo-activated localization microscopy
181 (sptPALM) under highly inclined and laminated optical sheet (HILO) illumination[11,16,33].
182 Using this setting, only a thin section of each cell surface that was close to the coverslip
183 was illuminated. To analyze the data, we only chose the fluorescent particles that
184 remained in focus for 4 - 12 frames (0.4 - 1.2 s). As free PAmCherry particles diffuse
185 extremely fast in the cytoplasm, entering and exiting the focal plane frequently, they
186 usually appear as blurry objects that cannot be followed at 10-Hz close to the
187 membrane[16]. For this reason, the noise from any potential degradation of AglR-
188 PAmCherry was negligible. Consistent with our previous results[11,14], 32.1% (n = 2,700) of
189 AglR-PAmCherry particles remained within one pixel (160 nm · 160 nm) before
190 photobleach, indicating that they were immotile. The remaining 67.9% AglR-
191 PAmCherry particles were motile, leaving trajectories of various lengths (**Fig. 4A, 4B**).

192 bFAC assembly is sensitive to mechanical cues. As the agar concentration increases

193 in gliding substrate, more motor molecules engage in bFACs, where they appear
194 immotile[9,11]. We exposed *aglR-PAmCherry* cells to 405-nm excitation (0.2 kW/cm^2) for 2 s,
195 where most PAmCherry molecules were photoactivated and used epifluorescence to
196 display the overall localization of AglR[11,16,30]. As the agar concentration increased,
197 bFACs increased significantly in size (**Fig. 4C**). Accordingly, the immotile AglR
198 particles detected by sptPALM increased from 10.7% (n = 1112) on 0.5% agar to 45.2% (n
199 = 726) on 5.0% agar surface (**Fig. 4B**). Thus, the stationary population of AglR-
200 PAmCherry particles reflects the AglR molecules in fully assembled bFACs.

201 In contrast to the cells that expressed wild-type AgmT (*agmT*$^+$), AglR particles were
202 hyper motile in the cells that lacked AgmT or expressed AgmT^{EAEA}. On 1.5% agar
203 surfaces, the immotile populations of AglR particles decreased to 10.5% (n = 2,989) and
204 11.7% (n = 1,408), respectively. Consistently, AglR-containing bFACs were rarely
205 detectable in these cells, even on 5% agar surfaces (**Fig. 4A-C**).

206 To test if other components in the gliding machinery also depend on AgmT to
207 assemble into bFACs, we tested the localization of AglZ, a cytoplasmic protein that is
208 commonly used for assessing bFAC assembly[10,34]. In the cells that expressed wild-type
209 AgmT, yellow fluorescent protein (YFP)-labeled AglZ formed a bright cluster at the
210 leading cell pole and multiple static, near-evenly spaced clusters along the cell body,
211 indicating the assembly of bFACs (**Fig. 4D**). In contrast, AglZ-YFP only formed single
212 clusters at cell poles in the cells that lacked AgmT or expressed AgmT^{EAEA} (**Fig. 4D**).
213 Taken together, the LTG activity of AgmT is essential for proper bFACs assembly.

214 **AgmT does not assemble into bFACs**

215 We first hypothesized that AgmT could assemble into bFACs, where it could generate
216 pores in PG specifically at bFAC loci that allow the inner and outer gliding complexes
217 interact directly. Alternatively, it could bind to PG and recruit other components to

218 bFACs through protein-protein interactions. Regardless, if AgmT assembles into
219 bFACs, it should localize in bFACs. To test this possibility, we labeled AgmT with
220 PAmCherry on its C-terminus and expressed the fusion protein as the sole source of
221 AgmT using the native promoter and locus of *agmT*. *agmT-PAmCherry pilA*$^{-}$ cells
222 displayed gliding motility that was indistinguishable from *pilA*$^{-}$ cells (**Fig. 2B**),
223 indicating that the fusion protein is functional. Similar to many membrane proteins that
224 resistant to dissociation by SDS[35], immunoblot using an anti-mCherry antibody showed
225 that AgmT-PAmCherry accumulated in two bands in SDS-PAGE that corresponded to
226 monomers and dimers of the full-length fusion protein, respectively (**Fig. 5A**). This
227 result is consistent with the structure of *E. coli* MltG that functions as homodimers
228 (PDB: 2r1f). Importantly, AgmT-PAmCherry was about 50 times more abundant than
229 AglR-PAmCherry (**Fig. 5A**). To test if AgmT assembles into bFACs, we first expressed
230 AgmT-PAmCherry and AglZ-YFP together using their respective loci and promoter.
231 We exposed *agmT-PAmCherry* cells to 405-nm excitation (0.2 kW/cm^2) for 2 s to visualize
232 the overall localization of AgmT. We found that on a 1.5% agar surface that favors
233 gliding motility, AglZ formed bright clusters at cell poles and aggregated in near
234 evenly-spaced bFACs along the cell body. In contrast, AgmT localized near evenly
235 along cell bodies without forming protein clusters (**Fig. 5B**). Thus, AgmT does not
236 localize into bFACs. These results echo the fact that despite its abundance, AgmT has
237 not been identified as a component in bFACs despite extensive pull-down experiments
238 using various bFAC components as baits[6,9,36].

239 As an additional test, we used sptPALM to track the movements of AgmT-
240 PAmCherry single particles on 1.5 agar surfaces at 10 Hz. We reasoned that if AgmT
241 assembles into bFACs, AgmT and gliding motors should display similar dynamic
242 patterns. Distinct from the AglR particles of which 32.1% remained stationary, AgmT
243 moved in a diffusive manner, showing no significant immotile population. Importantly,

244 compared to the diffusion coefficients (D) of motile AglR particles ($1.8 \cdot 10^{-2} \pm 3.6 \cdot 10^{-3}$
245 $\mu m^2/s$ (n = 1,833)), AgmT particles diffused much faster ($D = 2.9 \cdot 10^{-2} \pm 5.3 \cdot 10^{-3}$ $\mu m^2/s$ (n
246 = 8,548)). Taken together, AgmT and the gliding motor did not display significant
247 correlation in either their localization or dynamics. We thus conclude that AgmT does
248 not assemble into bFACs.

249 **AgmT connects bFACs to PG through its LTG activity**

250 We then explored the possibility that AgmT could modify PG through its LTG activity
251 and thus generate the anchor sites for certain components in bFACs. If this hypothesis is
252 true, heterologous expression of a non-native LTG could rescue gliding motility in the
253 *ΔagmT* strain. To test this hypothesis, we fused the *E. coli mltG* gene ($mltG_{Ec}$) to a
254 vanillate-inducible promoter and inserted the resulting construct to the *cuoA* locus on
255 *M. xanthus* chromosome that does not interfere gliding[37]. We subjected the *ΔagmT* and
256 $agmT^{EAEA}$ cells that expressed $MltG_{Ec}$ to mecillinam (100 μg/ml) stress. Induced by 200
257 μM sodium vanillate, $MltG_{Ec}$ restored cell morphology and integrity of the *ΔagmT* strain
258 to the wild-type level (**Fig. 3C**). This result confirmed that $MltG_{Ec}$ was expressed and
259 enzymatically active in *M. xanthus*. In contrast, $MltG_{Ec}$ failed to confer mecillinam
260 resistance to the $agmT^{EAEA}$ cells (**Fig. 3C**). A potential explanation is that $AgmT^{EAEA}$ could
261 still bind to PG and thus block $MltG_{Ec}$ from accessing *M. xanthus* PG.

262 Consistent with its LTG activity, the expression of $MltG_{Ec}$ restored gliding motility
263 of the *ΔagmT pilA*$^-$ cells on both the colony (**Fig. 2B**) and single-cell (**Fig. 2C, D**) levels.
264 Interestingly, in the absence of sodium vanillate, the leakage expression of $MltG_{Ec}$ using
265 the vanillate-inducible promoter was sufficient to compensate the loss of AgmT. A
266 plausible explanation of this observation is that as *E. coli* grows much faster (generation
267 time 20 - 30 min) than *M. xanthus* (generation time ~4 h), $MltG_{Ec}$ could possess
268 significantly higher LTG activity than AgmT. Induced by 200 μM sodium vanillate, the

269 expression of $MltG_{Ec}$ further but non significantly increased the velocity and gliding
270 persistency (**Fig. 2B-D**). Importantly, the expression of $MltG_{Ec}$ failed to restore gliding
271 motility in the *agmT*^{EAEA} *pilA* cells, even in the presence of 200 μM sodium vanillate (**Fig.**
272 **2B**). Consistent with the mecillinam resistance assay (**Fig. 3C**), this result suggests that
273 AgmT^{EAEA} still binds to PG and that in the absence of its LTG activity, AgmT does not
274 anchor bFACs to PG. As $MltG_{Ec}$ substitutes AgmT in gliding motility, it is the LTG
275 activity, rather than specific interactions between AgmT and bFACs, that is required for
276 gliding.

277 It is challenging to visualize how AgmT facilitates bFAC assembly through its
278 enzymatic activity *in vitro*. First, the inner complex in a bFAC spans the cytoplasm,
279 inner membrane, and periplasm and contains multiple proteins whose activities are
280 interdependent[8-10]. It is hence difficult to purify the entire inner complex in its functional
281 state. Second, Faure *et al*. hypothesized that AglQ and AglS in the gliding motor could
282 bind PG directly[10]. However, such binding has not been proved experimentally due to
283 the difficulty in purifying the membrane integral AglRQS complex. To overcome these
284 difficulties, we used AglR-PAmCherry to represent the inner complex of bFAC and
285 investigated how bFACs bind PG in their native environment. To do so, we expressed
286 AglR-PAmCherry in different genetic backgrounds as the sole source of AglR using the
287 native *aglR* locus and promoter. We lysed these cells using sonication, subjected their
288 lysates to centrifugation, isolated the pellets that contained PG, and detected the
289 presence of AglR-PAmCherry in these pellets by immunoblots using an mCherry
290 antibody. Eliminating AgmT and disabling its active site significantly reduced the
291 amounts of AglR in the pellets (**Fig. 5C**). Because such pellets contain both the PG and
292 membrane fractions, we further eliminated PG in cell lysates using lysozyme before
293 centrifugation and determined the amount of AglR-PAmCherry in the pellets that only
294 contained membrane fractions. Regardless of the presence and activity of AgmT,

295 comparable amounts of AglR precipitated in centrifugation pellets after lysozyme
296 treatment, indicating that AgmT does not affect the expression or stability of AglR (**Fig.**
297 **5C**). Thus, active AgmT facilitates the association between bFACs and PG. Strikingly,
298 the heterologous expression of $MltG_{Ec}$ enriched AglR-PAmCherry in the PG-containing
299 pellets from the *ΔagmT* cells but not the $agmT^{EAEA}$ ones (**Fig. 5C**). These results indicate
300 that AgmT connects bFACs to PG through its LTG activity.

301 The assembly of bFACs produces wave-like deformation on cell surface[6,38],
302 suggesting that their assembly may require a flexible PG layer[2,6,11,12]. As a major
303 contributor to cell stiffness, PG flexibility affects the overall stiffness of cells[39]. To test the
304 possibility that AgmT and $MltG_{Ec}$ facilitate bFAC assembly by reducing PG stiffness, we
305 adopted the GRABS assay[39] to quantify if the lack of AgmT and the expression of $MltG_{Ec}$
306 affects cell stiffness. To quantify changes in cell stiffness, we simultaneously measured
307 the growth of the $pilA^-$, *ΔagmT* $pilA^-$, and *ΔagmT* P_{van}-$MltG_{Ec}$ $pilA^-$ (with 200 μM sodium
308 vanillate) cells in a 1% agarose gel infused with CYE and liquid CYE and calculated the
309 GRABS scores of the *ΔagmT* $pilA^-$, and *ΔagmT* P_{van}-$MltG_{Ec}$ $pilA^-$ cells using the $pilA^-$ cells
310 as the reference, where positive and negative GRABS scores indicate increased and
311 decreased stiffness, respectively (see Materials and Methods and Ref[39]). The GRABS
312 scores of the *ΔagmT* $pilA^-$, and *ΔagmT* P_{van}-$MltG_{Ec}$ $pilA^-$ (with 200 μM sodium vanillate)
313 cells were -0.06 ± 0.04 and -0.10 ± 0.07 (n = 4), respectively, indicating that neither AgmT
314 nor $MltG_{Ec}$ affects cell stiffness significantly. Whereas PG flexibility could still be
315 essential for gliding, AgmT and $MltG_{Ec}$ do not regulate bFAC assembly by modulating
316 PG stiffness. Instead, these LTGs could connect bFACs to PG by generating structural
317 features that are irrelevant to PG stiffness.

318 **Discussion**

319 Gliding bacteria adopt a broad spectrum of nanomachineries. Compared to the trans-
320 envelope secretion system that drives gliding in *Flavobacterium johnsoniae* and
321 *Capnocytophaga gingivalis*, the gliding machinery of *M. xanthus* appears to lack a stable
322 structure that transverses the cell envelope, especially across the PG layer[2,40,41]. In order
323 to generate mechanical force from the fluid *M. xanthus* gliding machinery, the inner
324 complex must establish solid contact with PG and push the outer complex to slide[10,19]. In
325 this work, we discovered AgmT as the long-sought factor that facilitates persistent
326 gliding by connecting bFACs to PG.

327 It is surprising that AgmT itself does not assemble into bFACs and that $MltG_{Ec}$
328 substitutes AgmT in gliding. Thus, rather than interacting with bFAC components
329 directly and specifically, AgmT facilitates proper bFAC assembly indirectly through its
330 LTG activity. LTGs usually break glycan strands and produce unique anhydro caps on
331 their ends[42-46]. However, because AgmT is the only LTGs that is required for gliding, it
332 is not likely to facilitate bFAC assembly by generating such modification on glycan
333 strands. *E. coli* MltG is a glycan terminase that controls the length of newly synthesized
334 PG glycans[26]. Likewise, AgmT could generate short glycan strands and thus uniquely
335 modify the overall structure of *M. xanthus* PG, such as producing small pores that
336 retard and retain the inner subcomplexes of bFACs (**Fig. 6**). On the contrary, the *M.*
337 *xanthus* mutants that lack active AgmT could produce PG with increased strain length,
338 which blocks bFACs from binding to the cell wall and precludes stable bFAC assembly.
339 However, it would be very difficult to demonstrate how glycan length affects the
340 connection between bFACs and PG.

341 Then how does AgmT, a protein localized diffusively, facilitate bFAC assembly
342 into near-evenly spaced foci? The actin homolog MreB is the only protein in bFACs that

343 displays quasiperiodic localization independent of other components[16,21]. *M. xanthus*
344 MreB assembles into bFACs and positions the latter near evenly along the cell
345 body[6,11,16,21-23]. MreB filaments change their orientation in accordance with local
346 membrane curvatures and could hence respond to mechanical cues[47-49]. Strikingly, *M.*
347 *xanthus* does assemble bFACs in response to substrate hardness (**Fig. 4C**) and
348 assembled bFACs could distort the cell envelope, generating undulations on the cell
349 surface[6,9,11,38,50]. Taken together, whereas AgmT potentially modifies the entire PG layer,
350 it is still the quasiperiodic MreB filaments that determine the loci for bFAC assembly in
351 response to the mechanical cues from the gliding substrate (**Fig. 6**).

352 Most bacteria encode multiple LTGs that function in PG growth, remodeling, and
353 recycling[43,46]. This work provides an example that macro bacterial machineries
354 domesticate non-specialized LTGs for specialized functions. Other examples include
355 MltD in the *Helicobacter pylori* flagellum and MltE in the *E. coli* type VI secretion
356 system[51,52]. Based on their catalytic folds and domain arrangements, LTGs can be
357 categorized inti six distinct families[43]. Both *M. xanthus* AgmT and *E. coli* MltG belong to
358 the YceG/MltG family, which is the first identified LTG family that is conserved in both
359 Gram-negative and positive bacteria[26,43]. About 70% of bacterial genomes, including
360 firmicutes, proteobacteria, and actinobacteria, encode YceG/MltG domains[26]. The
361 unique inner membrane localization of this family and the fact that AgmT is the only *M.*
362 *xanthus* LTG that belongs to this family (**Table S2**) could partially explain why it is the
363 only LTG that contributes to gliding motility. It will be interesting to investigate if other
364 LTGs, once anchored to the inner membrane, could also facilitate force-generation by
365 bFACs.

366 **Methods**

367 **Strains and growth conditions**

368 *M. xanthus* strains used in this study are listed in **Table S2**. Vegetative *M. xanthus* cells
369 were grown in liquid CYE medium (10 mM MOPS pH 7.6, 1% (w/v) Bacto™ casitone
370 (BD Biosciences), 0.5% yeast extract and 8 mM $MgSO_4$) at 32 °C, in 125-ml flasks with
371 vigorous shaking, or on CYE plates that contains 1.5% agar. All genetic modifications
372 on *M. xanthus* were made on the chromosome. Deletion and insertion mutants were
373 constructed by electroporating *M. xanthus* cells with 4 μg of plasmid DNA.
374 Transformed cells were plated on CYE plates supplemented with 100 μg/ml sodium
375 kanamycin sulfate and 10 μg/ml tetracycline hydrochloride when needed. AgmT and
376 $AgmT^{EAEA}$ were labeled with PAmCherry at their C-termini by fusing their gene to a
377 DNA sequence that encodes PAmCherry through a KESGSVSSEQLAQFRSLD
378 (AAGGAGTCCGGCTCCGTGTCCTCCGAGCAGCTGGCCCAGTTCCGCTCCCTGGA
379 C) linker. All constructs were confirmed by PCR and DNA sequencing.

380 **Immunoblotting**

381 The expression and stability of PAmCherry-labeled proteins were determined by
382 immunoblotting following SDS-PAGE using an anti-mCherry antibody
383 (Rockland Immunochemicals, Inc., Lot 46705) and a goat anti-Rabbit IgG (H+L)
384 secondary antibody, HRP (Thermo Fisher Scientific, catalog # 31460). MreB was
385 detected as the loading control using an anti-MreB serum[21] and the same secondary
386 antibody. The blots were developed with Pierce™ ECL Western Blotting Substrate
387 (Thermo Fisher Scientific REF 32109) and a MINI-MED 90 processor (AFP
388 Manufacturing).

389 **Gliding assay**

390 Five microliters of cells from overnight culture were spotted on CYE plates containing
391 1.5% agar at 4 ×10^9 colony formation units (cfu)/ml and incubated at 32 °C for 48 h.
392 Colony edges were photographed using a Nikon Eclipse™ e600 phase-contrast
393 microscope with a 10× 0.30 NA objective and an OMAX™ A3590U camera.

394 **Protein expression and purification**

395 DNA sequences encoding amino acids 25 – 339 of AgmT and $AgmT^{EAEA}$ were amplified
396 by polymerase chain reaction (PCR) and inserted into the pET28a vector (Novogen)
397 between the restriction sites of *Eco*RI and *Hind*III and used to transform *E. coli* strain
398 BL21(DE3). Transformed cells were cultured in 20 ml LB (Luria-Bertani) broth at 37 °C
399 overnight and used to inoculate 1 L LB medium supplemented with 1.0% glucose.
400 Protein expression was induced by 0.1 mM IPTG (isopropyl-h-d-thiogalactopyranoside)
401 when the culture reached an OD_{600} of 0.8. Cultivation was continued at 16 °C for 10 h
402 before the cells were harvested by centrifugation at 6,000 × g for 20 min. Proteins were
403 purified using a NGC™ Chromatography System (BIO-RAD) and 5-ml HisTrap™
404 columns (Cytiva)[15,53]. Purified proteins were concentrated using Amicon™ Ultra
405 centrifugal filter units (Millipore Sigma) with a 10-kDa molecular weight cutoff and
406 stored at -80 °C.

407 **LTG activity (RBB) assay**

408 PG was purified following the published protocol[30,54]. In brief, *M. xanthus* cells were
409 grown until mid-stationary phase and harvested by centrifugation (6,000 × g, 20 min,
410 25 °C). Supernatant was discarded and the pellet was resuspended and boiled in 1× PBS
411 with 5% SDS for 2 h. SDS was removed by repetitive wash with water and
412 centrifugation (21,000 × g, 10 min, 25 °C). Purified PG from 100 ml culture was
413 suspended into 1 ml 1× PBS and stored at -20 °C. RBB labelling of PG was performed
414 essentially as previously described[28,29]. Purified sacculi were incubated with 20 mM RBB

415 in 0.25 M NaOH overnight at 37 °C. Reactions were neutralized by adding equal
416 volumes of 0.25 M HCl and RBB-labeled PG was collected by centrifugation at 21,000 ×
417 g for 15 min. Pellets were washed repeatedly with water until the supernatants became
418 colorless. RBB-labelled sacculi were incubated with purified AgmT and $AgmT^{EAEA}$ (1
419 mg/ml) at 25 °C for 12 h. lysozyme (1 mg/ml) was used as a positive control. Dye release
420 was quantified by the absorption at 595 nm from the supernatants after centrifugation
421 (21,000 × g, 10 min, 25 °C).

422 **Cell stiffness (GRABS) assay**

423 Cell stiffness was quantified using the GRABS assay[55]. Briefly, overnight cultures of
424 *pilA*$^-$, *ΔagmT pilA*$^-$, and *ΔagmT* P_{van}-$MltG_{Ec}$ *pilA*$^-$ (with 200 μM sodium vanillate) cells
425 were inoculated to liquid CYE medium or embedded in solid CYE medium with 1%
426 agarose to OD_{600} 0.5 in 2-ml optical spectrometer cuvettes and incubated at 32 °C.
427 Growth data were collected over 24 hr, and the GRABS scores were calculated as
428 $(OD_{mutant,\ agarose}/OD_{pilA,\ agarose})$ - $(OD_{mutant,\ liquid}/OD_{pilA,\ liquid})$.

429 **Co-precipitation assay**

430 *M. xanthus* cells expressing AglR-PAmCherry were grown in liquid CYE to OD_{600} ~1,
431 harvested by centrifugation (6,000 × g, 20 min, 25 °C), washed by 1× PBS, and
432 resuspended into 1× PBS to OD_{600} 6. Cells (1 ml) were lysed using a Cole-Parmer 4710
433 Ultrasonic Homogenizer. Unbroken cells and large debris were eliminated by
434 centrifugation (6,000 × g, 10 min, 25 °C). Supernatants were subjected to centrifugation
435 at 21,000 × g for 15 min. Pellets that contain both the PG and membrane fractions were
436 resuspended to 1 ml in 1× PBS. To collect the pellets that do not contain PG,
437 supernatants from sonication lysates were incubated with 5 mg/ml lysozyme at 25 °C
438 for 5 h before centrifugation. Five microliters of each resuspended pellet were mixed

439 with 5 μl 2× loading buffer and applied to SDS-PAGE. AglR-PAmCherry was detected
440 using immunoblotting.

441 **Microscopy Analysis**

442 For all imaging experiments, we spotted 5 μl of cells grown in liquid CYE medium to
443 OD_{600} ~1 on agar (1.5%) pads. For the treatments with inhibitors, inhibitors were added
444 into both the cell suspension and agar pads. The length and width of cells were
445 determined from differential interference contrast (DIC) images using a MATLAB
446 (MathWorks) script[16,30,56]. DIC and fluorescence images of cells were captured using an
447 Andor iXon Ultra 897 EMCCD camera (effective pixel size 160 nm) on an inverted
448 Nikon Eclipse-Ti™ microscope with a 100× 1.49 NA TIRF objective. For sptPALM, *M.*
449 *xanthus* cells were grown in CYE to 4×10^8 cfu/ml and PAmCherry was activated using a
450 405-nm laser (0.3 kW/cm^2), excited and imaged using a 561-nm laser (0.2 kW/cm^2).
451 Images were acquired at 10 Hz. For each sptPALM experiment, single PAmCherry
452 particles were localized in at least 100 individual cells from three biological replicates.
453 sptPALM data were analyzed using a MATLAB (MathWorks) script[16,56]. Briefly, cells
454 were identified using differential interference contrast images. Single PAmCherry
455 particles inside cells were fit by a symmetric 2D Gaussian function, whose center was
456 assumed to be the particle's position[16]. Particles that explored areas smaller than 160 nm
457 × 160 nm (within one pixel) in 0.4 - 1.2 s were considered immotile[16,30,56]. Sample
458 trajectories were generated using the TrackMate[57] plugin in the ImageJ suite
459 (https://imagej.net).

Acknowledgements

We thank the Department of Biology and the College of Arts and Sciences at Texas A&M University for the support on camera purchase. This work is supported by the National Institute of Health R01GM129000 to B. N.. C. A. R. C. was supported in the 2023 – 2024 academic year by a National Institute of Health Diverse Predoctoral Training in Genetics grant T32GM135115 awarded to the Genetics and Genomics Interdisciplinary Program at Texas A&M University.

Author Contributions

C. R. C., O. G. F., and B. N. designed the study, performed experiments and data analysis, and wrote the manuscript. All authors read and approved the manuscript.

Competing Interests

The authors declare no competing interests.

Data availability

All data generated or analyzed during this study are included in the manuscript and supporting files.

References

1 Laventie, B. J. & Jenal, U. Surface Sensing and Adaptation in Bacteria. *Annu Rev Microbiol* **74**, 735-760 (2020). https://doi.org/10.1146/annurev-micro-012120-063427

2 Nan, B. & Zusman, D. R. Novel mechanisms power bacterial gliding motility. *Mol Microbiol* **101**, 186-193 (2016). https://doi.org/10.1111/mmi.13389

3 Chang, Y. W. *et al.* Architecture of the type IVa pilus machine. *Science* **351**, aad2001 (2016). https://doi.org/10.1126/science.aad2001

4 Wu, S. S. & Kaiser, D. Genetic and functional evidence that Type IV pili are required for social gliding motility in *Myxococcus xanthus*. *Mol Microbiol* **18**, 547-558 (1995).

5 Nan, B. & Zusman, D. R. Uncovering the mystery of gliding motility in the myxobacteria. *Annu Rev Genet* **45**, 21-39 (2011). https://doi.org/10.1146/annurev-genet-110410-132547

6 Nan, B. *et al.* Myxobacteria gliding motility requires cytoskeleton rotation powered by proton motive force. *Proc Natl Acad Sci U S A* **108**, 2498-2503 (2011). https://doi.org/10.1073/pnas.1018556108

7 Sun, M., Wartel, M., Cascales, E., Shaevitz, J. W. & Mignot, T. Motor-driven intracellular transport powers bacterial gliding motility. *Proc Natl Acad Sci U S A* **108**, 7559-7564 (2011). https://doi.org/1101101108 [pii] 10.1073/pnas.1101101108

8 Jakobczak, B., Keilberg, D., Wuichet, K. & Sogaard-Andersen, L. Contact- and Protein Transfer-Dependent Stimulation of Assembly of the Gliding Motility Machinery in *Myxococcus xanthus*. *PLoS Genet* **11**, e1005341 (2015). https://doi.org/10.1371/journal.pgen.1005341

9 Nan, B., Mauriello, E. M., Sun, I. H., Wong, A. & Zusman, D. R. A multi-protein complex from *Myxococcus xanthus* required for bacterial gliding motility. *Mol Microbiol* **76**, 1539-1554 (2010). https://doi.org/10.1111/j.1365-2958.2010.07184.x

10 Faure, L. M. *et al.* The mechanism of force transmission at bacterial focal adhesion complexes. *Nature* **539**, 530-535 (2016). https://doi.org/10.1038/nature20121

11 Nan, B. *et al.* Flagella stator homologs function as motors for myxobacterial gliding motility by moving in helical trajectories. *Proc Natl Acad Sci U S A* **110**, E1508-1513 (2013). https://doi.org/10.1073/pnas.1219982110

12 Nan, B., McBride, M. J., Chen, J., Zusman, D. R. & Oster, G. Bacteria that glide with helical tracks. *Curr Biol* **24**, R169-R173 (2014). https://doi.org/10.1016/j.cub.2013.12.034

13 Nan, B. Bacterial Gliding Motility: Rolling Out a Consensus Model. *Curr Biol* **27**, R154-R156 (2017). https://doi.org/10.1016/j.cub.2016.12.035

14 Nan, B. *et al.* The polarity of myxobacterial gliding is regulated by direct interactions between the gliding motors and the Ras homolog MglA. *Proc Natl Acad Sci U S A* **112**, E186-193 (2015). https://doi.org/10.1073/pnas.1421073112

15 Pogue, C. B., Zhou, T. & Nan, B. PlpA, a PilZ-like protein, regulates directed motility of the bacterium *Myxococcus xanthus*. *Mol Microbiol* **107**, 214-228 (2018). https://doi.org/10.1111/mmi.13878

16 Fu, G. *et al.* MotAB-like machinery drives the movement of MreB filaments during bacterial gliding motility. *Proc Natl Acad Sci U S A* **115**, 2484-2489 (2018). https://doi.org/10.1073/pnas.1716441115

17 Garner, E. C. Toward a Mechanistic Understanding of Bacterial Rod Shape Formation and Regulation. *Annu Rev Cell Dev Biol* **37**, 1-21 (2021). https://doi.org/10.1146/annurev-cellbio-010521-010834

18 Rohs, P. D. A. & Bernhardt, T. G. Growth and Division of the Peptidoglycan Matrix. *Annu Rev Microbiol* **75**, 315-336 (2021). https://doi.org/10.1146/annurev-micro-020518-120056

19 Chen, J. & Nan, B. Flagellar Motor Transformed: Biophysical Perspectives of the *Myxococcus xanthus* Gliding Mechanism. *Front Microbiol* **13**, 891694 (2022). https://doi.org/10.3389/fmicb.2022.891694

20 Zhang, H., Venkatesan, S. & Nan, B. Y. *Myxococcus xanthus* as a Model Organism for Peptidoglycan Assembly and Bacterial Morphogenesis. *Microorganisms* **9** (2021). https://doi.org/10.3390/microorganisms9050916

21 Mauriello, E. M. *et al.* Bacterial motility complexes require the actin-like protein, MreB and the Ras homologue, MglA. *Embo J* **29**, 315-326 (2010). https://doi.org/10.1038/emboj.2009.356

22 Treuner-Lange, A. *et al.* The small G-protein MglA connects to the MreB actin cytoskeleton at bacterial focal adhesions. *J Cell Biol* **210**, 243-256 (2015). https://doi.org/10.1083/jcb.201412047

23 Zhang, H. *et al.* Establishing rod shape from spherical, peptidoglycan-deficient bacterial spores. *Proc Natl Acad Sci U S A* **117**, 14444-14452 (2020). https://doi.org/10.1073/pnas.2001384117

24 Youderian, P., Burke, N., White, D. J. & Hartzell, P. L. Identification of genes required for adventurous gliding motility in *Myxococcus xanthus* with the transposable element mariner. *Mol Microbiol* **49**, 555-570 (2003).

25 Aramayo, R. & Nan, B. *De Novo* Assembly and Annotation of the Complete Genome Sequence of *Myxococcus xanthus* DZ2. *Microbiol Resour Announc*, e0107421 (2022). https://doi.org/10.1128/mra.01074-21

26 Yunck, R., Cho, H. & Bernhardt, T. G. Identification of MltG as a potential terminase for peptidoglycan polymerization in bacteria. *Mol Microbiol* **99**, 700-718 (2016). https://doi.org/10.1111/mmi.13258

27 Leonardy, S. *et al.* Regulation of dynamic polarity switching in bacteria by a Ras-like G-protein and its cognate GAP. *Embo J* **29**, 2276-2289 (2010). https://doi.org/10.1038/emboj.2010.114

28 Uehara, T., Parzych, K. R., Dinh, T. & Bernhardt, T. G. Daughter cell separation is controlled by cytokinetic ring-activated cell wall hydrolysis. *EMBO J* **29**, 1412-1422 (2010). https://doi.org/10.1038/emboj.2010.36

29 Jorgenson, M. A., Chen, Y., Yahashiri, A., Popham, D. L. & Weiss, D. S. The bacterial septal ring protein RlpA is a lytic transglycosylase that contributes to rod shape and daughter cell separation in *Pseudomonas aeruginosa*. *Mol Microbiol* **93**, 113-128 (2014). https://doi.org/10.1111/mmi.12643

30 Zhang, H., Venkatesan, S., Ng, E. & Nan, B. Coordinated peptidoglycan synthases and hydrolases stabilize the bacterial cell wall. *Nature communications* **14**, 5357 (2023). https://doi.org/10.1038/s41467-023-41082-3

562 31 Weaver, A. I. *et al.* Lytic transglycosylases mitigate periplasmic crowding by degrading
563 soluble cell wall turnover products. *Elife* **11** (2022). https://doi.org/10.7554/eLife.73178
564 32 Cho, H., Uehara, T. & Bernhardt, T. G. Beta-lactam antibiotics induce a lethal
565 malfunctioning of the bacterial cell wall synthesis machinery. *Cell* **159**, 1300-1311 (2014).
566 https://doi.org/10.1016/j.cell.2014.11.017
567 33 Tokunaga, M., Imamoto, N. & Sakata-Sogawa, K. Highly inclined thin illumination
568 enables clear single-molecule imaging in cells. *Nat Methods* **5**, 159-161 (2008).
569 https://doi.org/10.1038/nmeth1171
570 34 Mignot, T., Shaevitz, J. W., Hartzell, P. L. & Zusman, D. R. Evidence that focal adhesion
571 complexes power bacterial gliding motility. *Science* **315**, 853-856 (2007).
572 35 Rath, A., Glibowicka, M., Nadeau, V. G., Chen, G. & Deber, C. M. Detergent binding
573 explains anomalous SDS-PAGE migration of membrane proteins. *Proc Natl Acad Sci U S*
574 *A* **106**, 1760-1765 (2009). https://doi.org/10.1073/pnas.0813167106
575 36 Jolivet, N. Y. *et al.* Integrin-like adhesin CglD confers traction and stabilizes bacterial focal
576 adhesions involved in myxobacterial gliding motility. *bioRxiv*, 2023.2010.2019.562135
577 (2023). https://doi.org/10.1101/2023.10.19.562135
578 37 Iniesta, A. A., Garcia-Heras, F., Abellon-Ruiz, J., Gallego-Garcia, A. & Elias-Arnanz, M.
579 Two systems for conditional gene expression in *Myxococcus xanthus* inducible by
580 isopropyl-beta-D-thiogalactopyranoside or vanillate. *J Bacteriol* **194**, 5875-5885 (2012).
581 https://doi.org/10.1128/JB.01110-12
582 38 Tchoufag, J., Ghosh, P., Pogue, C. B., Nan, B. & Mandadapu, K. K. Mechanisms for
583 bacterial gliding motility on soft substrates. *Proc Natl Acad Sci U S A* **116**, 25087-25096
584 (2019). https://doi.org/10.1073/pnas.1914678116
585 39 Auer, G. K. *et al.* Mechanical Genomics Identifies Diverse Modulators of Bacterial Cell
586 Stiffness. *Cell Syst* **2**, 402-411 (2016). https://doi.org/10.1016/j.cels.2016.05.006
587 40 James, R. H. *et al.* Structure and mechanism of the proton-driven motor that powers type
588 9 secretion and gliding motility. *Nature Microbiology* **6**, 221-+ (2021).
589 https://doi.org/10.1038/s41564-020-00823-6
590 41 Shrivastava, A. *et al.* Cargo transport shapes the spatial organization of a microbial
591 community. *Proc Natl Acad Sci U S A* **115**, 8633-8638 (2018).
592 https://doi.org/10.1073/pnas.1808966115
593 42 Williams, A. H. *et al.* A step-by-step in crystallo guide to bond cleavage and 1,6-anhydro-
594 sugar product synthesis by a peptidoglycan-degrading lytic transglycosylase. *J Biol Chem*
595 **293**, 6000-6010 (2018). https://doi.org/10.1074/jbc.RA117.001095
596 43 Dik, D. A., Marous, D. R., Fisher, J. F. & Mobashery, S. Lytic transglycosylases: concinnity
597 in concision of the bacterial cell wall. *Crit Rev Biochem Mol Biol* **52**, 503-542 (2017).
598 https://doi.org/10.1080/10409238.2017.1337705
599 44 Holtje, J. V., Mirelman, D., Sharon, N. & Schwarz, U. Novel type of murein
600 transglycosylase in *Escherichia coli*. *J Bacteriol* **124**, 1067-1076 (1975).
601 https://doi.org/10.1128/jb.124.3.1067-1076.1975
602 45 van Heijenoort, J. Peptidoglycan hydrolases of *Escherichia coli*. *Microbiol Mol Biol Rev* **75**,
603 636-663 (2011). https://doi.org/10.1128/MMBR.00022-11

604 46 Weaver, A., Taguchi, A. & Dorr, T. Masters of Misdirection: Peptidoglycan Glycosidases
605 in Bacterial Growth. *J Bacteriol* **205**, e0042822 (2023). https://doi.org/10.1128/jb.00428-22
606 47 Hussain, S. *et al.* MreB filaments align along greatest principal membrane curvature to
607 orient cell wall synthesis. *Elife* **7** (2018). https://doi.org/10.7554/eLife.32471
608 48 Wong, F., Garner, E. C. & Amir, A. Mechanics and dynamics of translocating MreB
609 filaments on curved membranes. *Elife* **8** (2019). https://doi.org/10.7554/eLife.40472
610 49 Ursell, T. S. *et al.* Rod-like bacterial shape is maintained by feedback between cell
611 curvature and cytoskeletal localization. *Proc Natl Acad Sci U S A* **111**, E1025-1034 (2014).
612 https://doi.org/10.1073/pnas.1317174111
613 50 Chen, Y., Topo, E. J., Nan, B. & Chen, J. Mathematical modeling of mechanosensitive
614 reversal control in *Myxococcus xanthus*. *Front Microbiol* **14**, 1294631 (2023).
615 https://doi.org/10.3389/fmicb.2023.1294631
616 51 Roure, S. *et al.* Peptidoglycan maturation enzymes affect flagellar functionality in bacteria.
617 *Mol Microbiol* **86**, 845-856 (2012). https://doi.org/10.1111/mmi.12019
618 52 Santin, Y. G. & Cascales, E. Domestication of a housekeeping transglycosylase for
619 assembly of a Type VI secretion system. *EMBO Rep* **18**, 138-149 (2017).
620 https://doi.org/10.15252/embr.201643206
621 53 Nan, B. *et al.* Purification and preliminary X-ray crystallographic analysis of the ligand-
622 binding domain of *Sinorhizobium meliloti* DctB. *Biochim Biophys Acta* **1764**, 839-841 (2006).
623 https://doi.org/10.1016/j.bbapap.2005.10.023
624 54 Alvarez, L., Hernandez, S. B., de Pedro, M. A. & Cava, F. Ultra-Sensitive, High-Resolution
625 Liquid Chromatography Methods for the High-Throughput Quantitative Analysis of
626 Bacterial Cell Wall Chemistry and Structure. *Methods Mol Biol* **1440**, 11-27 (2016).
627 https://doi.org/10.1007/978-1-4939-3676-2_2
628 55 Adan-Kubo, J., Uenoyama, A., Arata, T. & Miyata, M. Morphology of isolated Gli349, a
629 leg protein responsible for *Mycoplasma mobile* gliding via glass binding, revealed by rotary
630 shadowing electron microscopy. *J Bacteriol* **188**, 2821-2828 (2006).
631 https://doi.org/10.1128/JB.188.8.2821-2828.2006
632 56 Zhang, H., Venkatesan, S., Ng, E. & Nan, B. Coordinated peptidoglycan synthases and
633 hydrolases stabilize the bacterial cell wall. *GitHub* (2023).
634 https://doi.org/10.5281/zenodo.8234126
635 57 Ershov, D. *et al.* TrackMate 7: integrating state-of-the-art segmentation algorithms into
636 tracking pipelines. *Nat Methods* **19**, 829-832 (2022). https://doi.org/10.1038/s41592-022-
637 01507-1

638

639 **Figure legends**

640 **Fig. 1. Stationary bFACs drive *M. xanthus* gliding.** Motors carrying incomplete
641 gliding complexes either diffuse or move rapidly along helical paths but do not generate
642 propulsion. Motors stall and become nearly static relative to the substrate when they
643 assemble into complete bFACs with other motor-associated proteins at the ventral side
644 of the cell. Stalled motors push MreB and bFACs in opposite directions and thus exert
645 force against outer membrane adhesins. Overall, as motors transport bFACs toward
646 lagging cell poles, cells move forward but bFACs remain static relative to the substrate.
647 IM, inner membrane; OM, outer membrane.

648 **Fig. 2. AgmT, a putative lytic transglycosylase, is required *for M. xanthus* gliding.**
649 **A)** AgmT shows significant similarity to a widely conserved PG transglycosylase in
650 YceG/MltG family. The conserved glutamine residue is marked by an asterisk. M_xant,
651 *M. xanthus*; E_coli, *E. coli*; M_tube, *Mycobacterium tuberculosis*; S_coel, *Streptomyces*
652 *coelicolor*; A_calc, *Acinetobacter calcoaceticus*; X_albi, *Xanthomonas albilineans*;
653 N_meni, *Neisseria meningitidis*; R_prow, *Rickettsia prowazekii*; T_aqua, *Thermus*
654 *aquaticus*. **B)** AgmT is required for *M. xanthus* gliding. Colony edges were imaged after
655 incubating cells on 1.5% agar surface for 24 h. To eliminate S-motility, we further
656 knocked out the *pilA* gene that encodes pilin for type IV pilus. Cells that move by gliding
657 are able to move away from colony edges. Deleting *agmT* or disabling the active site of
658 AgmT abolish gliding but fusing an PAmCherry (PAmCh) to its C-terminus does not.
659 Heterologous Expression of *E. coli* MltG ($MltG_{Ec}$) restores gliding of *agmT* cells but not
660 the cells that express $AgmT^{EAEA}$. **C, D)** While cells lacking AgmT moved slower **(C)** and
661 less persistently (**D**, measured by the distances cells traveled before pauses and
662 reversals), the expression of $MltG_{Ec}$ restores both the velocity and persistence of gliding
663 in the *agmT* cells. Data were pooled from three independent experiments and *p* values
664 were calculated using a one-way ANOVA test between two unweighted, independent
665 samples. Boxes indicate the 25th - 75th percentiles and bars the median. The total
666 number of cells analyzed is shown on top of each plot. *, p <0.001.

667 **Fig. 3. AgmT regulates cell morphology and integrity under antibiotic stress. A)**
668 Purified AgmT solubilizes dye-labeled PG sacculi, but $AgmT^{EAEA}$ does not. Lysozyme

669 serves as a positive control. Absorption at 595 nm was measured after 18 h incubation
670 at 25 C. Data are presented as mean values ± SD from three replicates. **B)** AgmT
671 regulates cell morphology. Compared to wild-type cells, cells that lack AgmT and
672 express AgmT^{EAEA} are significantly shorter and wider. A previously reported mutant that
673 lacks all three class A penicillin-binding proteins (*Δ3*) displays similarly shortened and
674 widened morphology but is still motile by gliding (**Fig. S1**). Heterologous expression of
675 *E. coli* MltG partially restores cell length but not cell width in *agmT* and *agmT^{EAEA}*
676 backgrounds. Asterisks, 200 M sodium vanillate added. *p* values were calculated using
677 a one-way ANOVA test between two unweighted, independent samples. Whiskers
678 indicate the 25th - 75th percentiles and red dots the median. The total number of cells
679 analyzed is shown on top of each plot. **C)** AgmT regulates cell morphology and integrity
680 under mecillinam stress (100 µg/ml). Expressing *E. coli* MltG by a vanillate-inducible
681 promoter (P_{van}) restores resistance against mecillinam in *agmT* cells but not in the cells
682 that express AgmT^{EAEA}. van, 200 M sodium vanillate. Arrows point to newly lysed cells.
683 Scale bars, 5 µm.

684 **Fig. 4. AgmT and its LTG activity are essential for proper bFAC assembly. A)**
685 Overall distribution of AglR-PAmCherry particles on 1.5% agar surface is displayed
686 using the composite of 100 consecutive frames taken at 100-ms intervals. Single-
687 particle trajectories of AglR-PAmCherry (AglR-PAmCh) were generated from the same
688 frames. Individual trajectories are distinguished by colors. Deleting *agmT* or disabling
689 the transglycosylase activity of AgmT (AgmT^{EAEA}) decrease the stationary population of
690 AglR particles. **B)** The stationary population of AglR-PAmCherry particles, which reflects
691 the AglR molecules in bFACs, changes in response to substrate hardness (controlled by
692 agar concentration) and the presence and function of AgmT. The total number of
693 particles analyzed is shown on top of each plot. **C)** AglR fails to assemble into bFACs in
694 the absence of active AgmT, even on 5.0% agar surfaces. **D)** AgmT and its LTG activity
695 also support the assembly of AglZ into bFACs. White arrows point to bFACs. Scale
696 bars, 5 µm.

697 **Fig. 5. AgmT does not assemble into bFACs but connects bFACs to PG. A)**
698 Immunoblotting using *M. xanthus* cell lysates and an anti-mCherry antibody shows that

699 PAmCherry (PAmCh)-labeled AgmT and AgmT^{EAEA} (592 amino acids) accumulate as
700 full-length proteins. AgmT is significantly more abundant than the PAmCherry-labeled
701 motor protein AglR (498 amino acids). The bacterial actin homolog MreB visualized
702 using an MreB antibody is shown as a loading control. **B)** AgmT does not aggregate into
703 bFACs. **C)** The LTG activity of AgmT is required for connecting bFACs to PG and
704 expressing the *E. coli* LTG MltG ($MltG_{Ec}$) restores PG binding by bFACs in cells that
705 lack AgmT but not in the ones that express an inactive AgmT variant (AgmT^{EAEA}). AglR-
706 PAmCherry was detected using an anti-mCherry antibody to mark the presence of
707 bFACs that co-precipitate with PG-containing (lysozyme-) pellets. Lysates from the cells
708 that express AglR-PAmCherry in different genetic backgrounds were pelleted by
709 centrifugation in the presence and absence of lysozyme. The loading control of AglR-
710 PAmCherry in the whole cell is shown as “total”.

711 **Fig. 6. A possible mechanism by which AgmT connect bFACs to PG.** AgmT could
712 generate short glycan strands through its LTG activity and thus uniquely modify the
713 overall structure of *M. xanthus* PG, such as producing small pores that retard and retain
714 the inner subcomplexes of bFACs. Likewise, the *M. xanthus* mutants that lack active
715 AgmT could produce PG with increased strain length, which precludes bFACs from
716 binding to the cell wall.

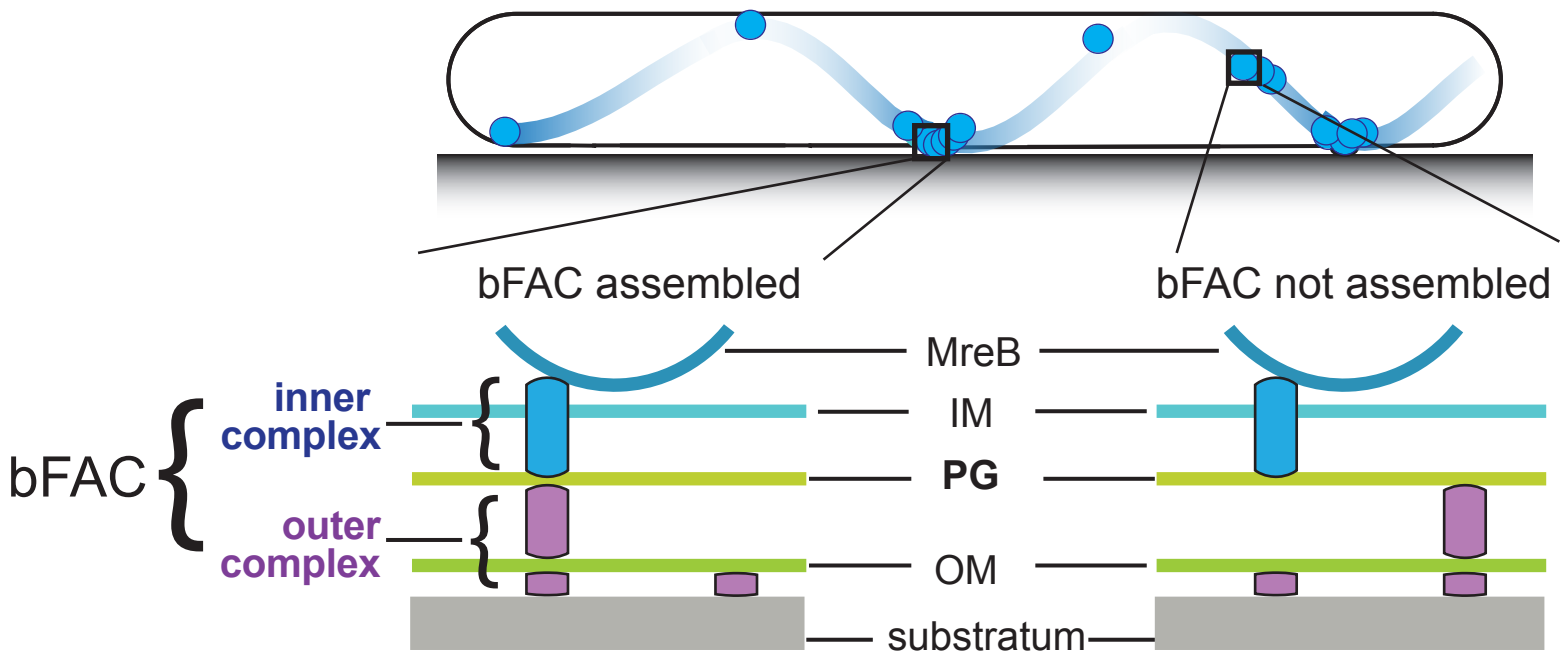
bFAC assembled
bFAC not assembled
MreB
IM
PG
OM
substratum
bFAC
inner complex
outer complex

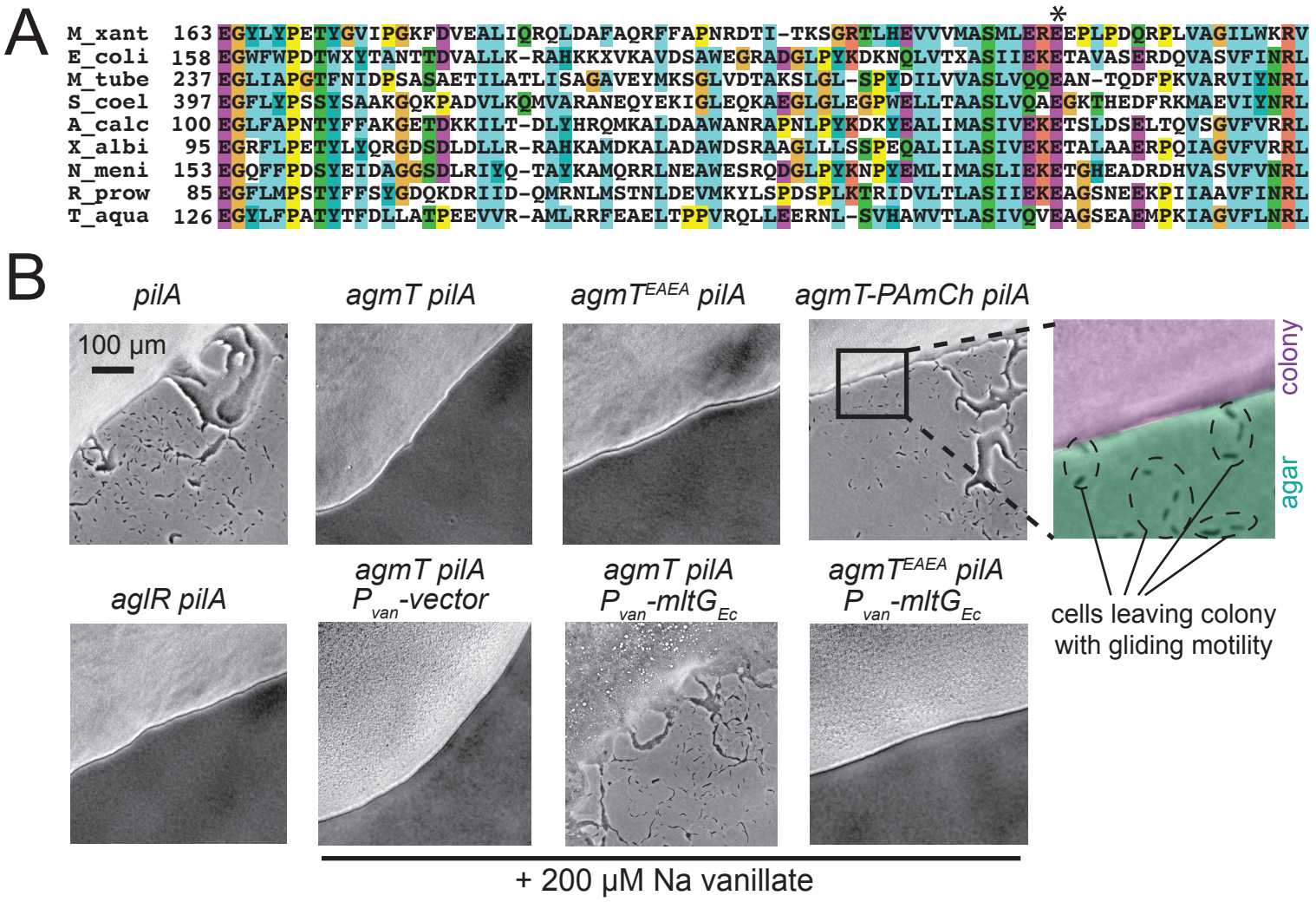
A
M_xant 163 EGYLYPETYGVIPGKFDVEALIQRQLDAFAQRFFAPNRDTI-TKSGRTLHEVVVMASMLEREEPLPDQRPLVAGILWKRV
E_coli 158 EGWFWPDTWXYTANTTDVALLK-RAHKKXVKAVDSAWEGRADGLPYKDKNQLVTXASIIEKETAVASERDQVASVFINRL
M_tube 237 EGLIAPGTFNIDPSASAETILATLISAGAVEYMKSGLVDTAKSLGL-SPYDILVVASLVQQEAN-TQDFPKVARVIYNRL
S_coel 397 EGFLYPSSYSAAKGQKPADVLKQMVARANEQYEKIGLEQKAEGLGLEGPWELLTAASLVQAEGKTHEDFRKMAEVIYNRL
A_calc 100 EGLFAPNTYFFAKGETDKKILT-DLYHRQMKALDAAWANRAPNLPYKDKYEALIMASIVEKETSLDSELTQVSGVFVRRL
X_albi 95 EGRFLPETYLYQRGDSDLDLLR-RAHKAMDKALADAWDSRAAGLLLSSPEQALILASIVEKETALAAERPQIAGVFVRRL
N_meni 153 EGQFFPDSYEIDAGGSDLRIYQ-TAYKAMQRRLNEAWESRQDGLPYKNPYEMLIMASLIEKETGHEADRDHVASVFVNRL
R_prow 85 EGFLMPSTYFFSYGDQKDRIID-QMRNLMSTNLDEVMKYLSPDSPLKTRIDVLTLASIIEKEAGSNEEKPIIAAVFINRL
T_aqua 126 EGYLFPATYTFDLLATPEEVVR-AMLRRFEAELTPPVRQLLEERNL-SVHAWVTLASIVQVEAGSEAEMPKIAGVFLNRL
B
pilA
agmT pilA
agmT^EAEA pilA
agmT-PAmCh pilA
100 µm
colony
agar
cells leaving colony with gliding motility
aglR pilA
agmT pilA P_van-vector
agmT pilA P_van-mltG_Ec
agmT^EAEA pilA P_van-mltG_Ec
+ 200 µM Na vanillate
C
Velocity (µm/min)
p = 0.07
46
59
44
51
pilA
agmT pilA
agmT pilA P_van-mltG_EC 0 µM vanillate
agmT pilA P_van-mltG_EC 200 µM vanillate
D
Gliding persistency (µm)
p = 0.67
46
59
44
51
pilA
agmT pilA
agmT pilA P_van-mltG_EC 0 µM vanillate
agmT pilA P_van-mltG_EC 200 µM vanillate

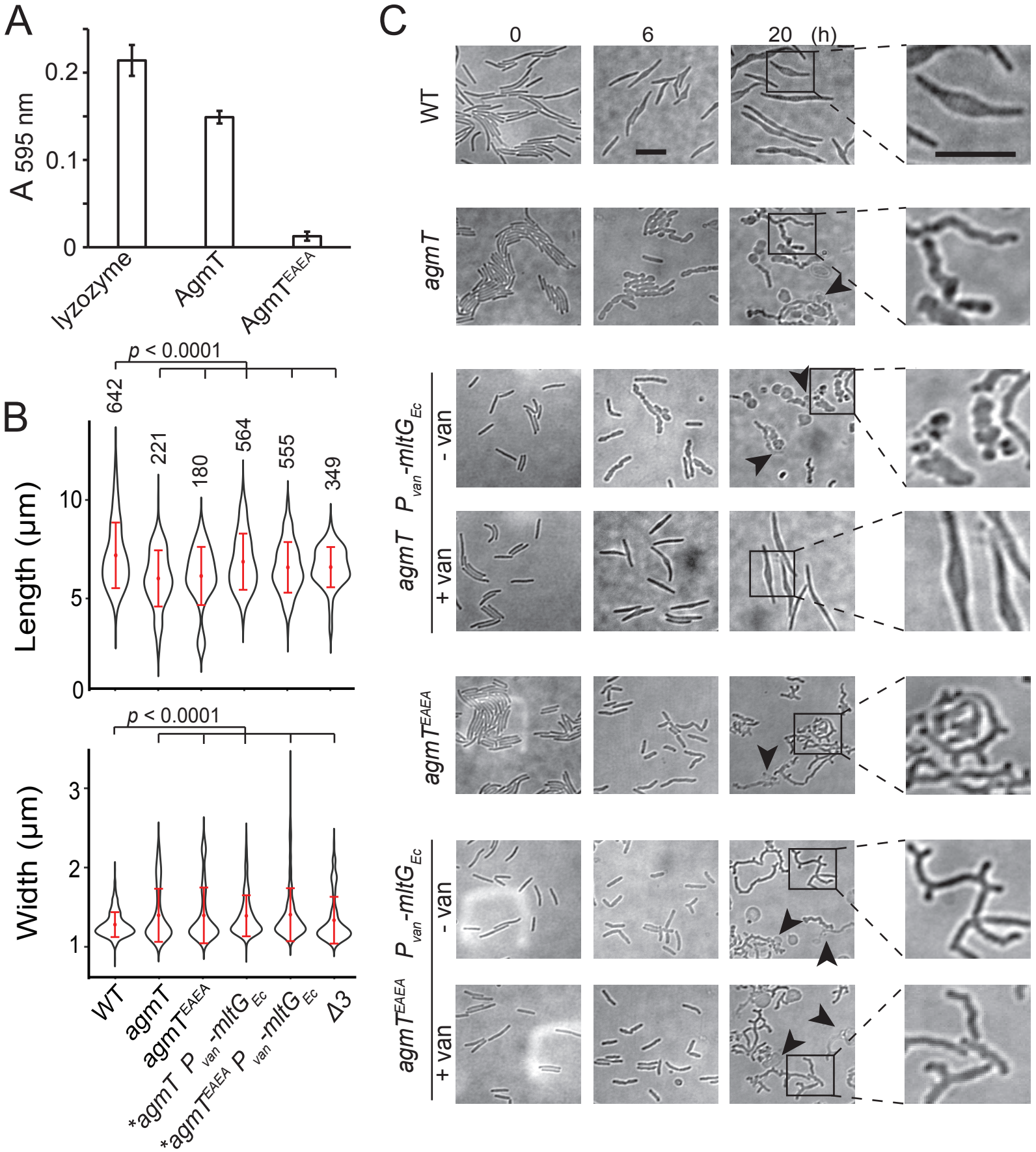
A
A 595 nm
0.2
0.1
0
lyzozyme
AgmT
AgmT^EAEA
B
p < 0.0001
642
221
180
564
555
349
Length (µm)
10
5
0
p < 0.0001
Width (µm)
3
2
1
WT
agmT
agmT^EAEA
*agmT P_van-mltG_Ec
*agmT^EAEA P_van-mltG_Ec
Δ3
C
0
6
20 (h)
WT
agmT
agmT P_van-mltG_Ec
- van
+ van
agmT^EAEA
agmT^EAEA P_van-mltG_Ec
- van
+ van

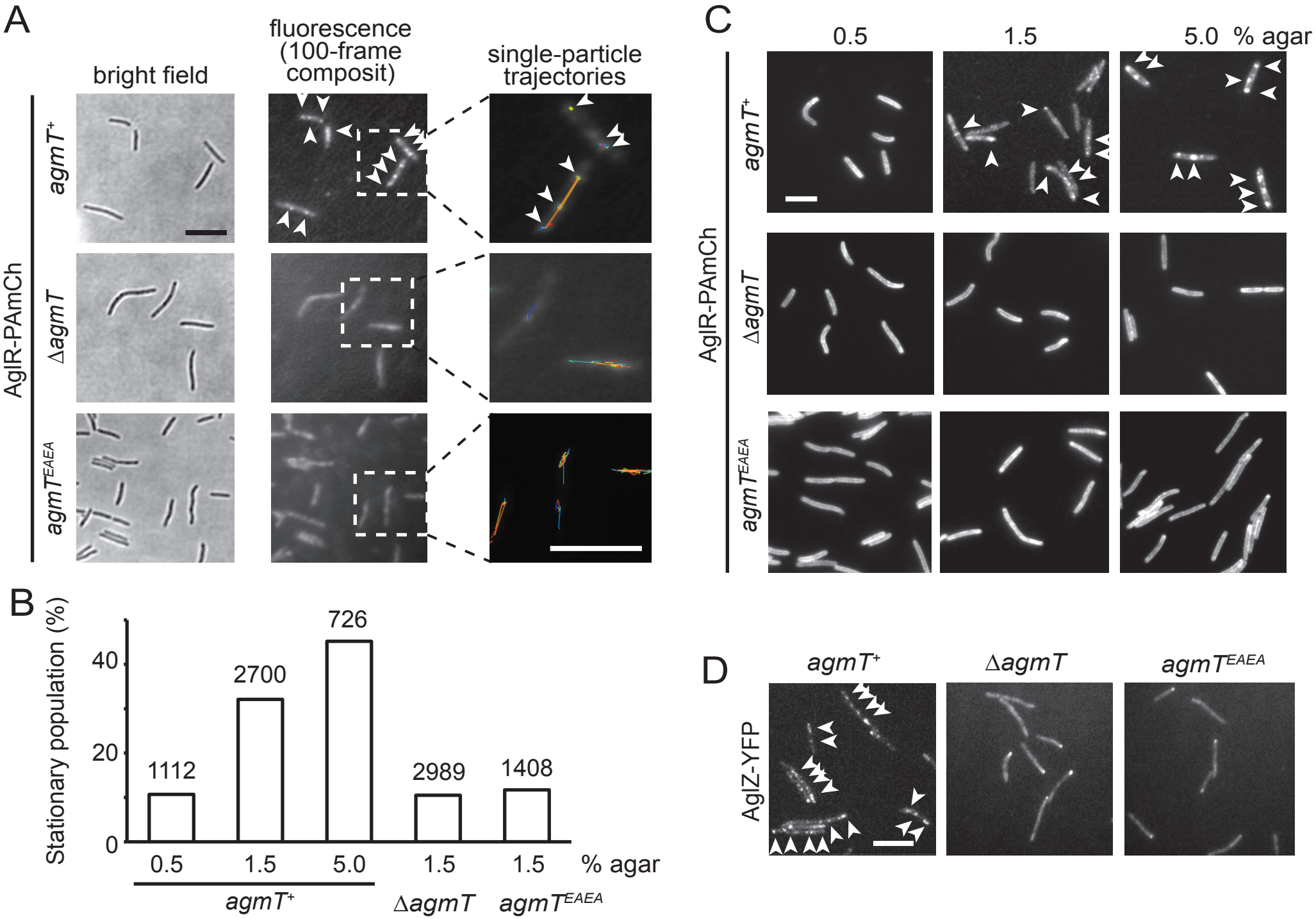
A
bright field
fluorescence (100-frame composit)
single-particle trajectories
AglR-PAmCh
agmT+
ΔagmT
agmTEAEA
B
Stationary population (%)
0
20
40
1112
2700
726
2989
1408
0.5
1.5
5.0
1.5
1.5
% agar
agmT+
ΔagmT
agmTEAEA
C
0.5
1.5
5.0 % agar
AglR-PAmCh
agmT+
ΔagmT
agmTEAEA
D
agmT+
ΔagmT
agmTEAEA
AglZ-YFP

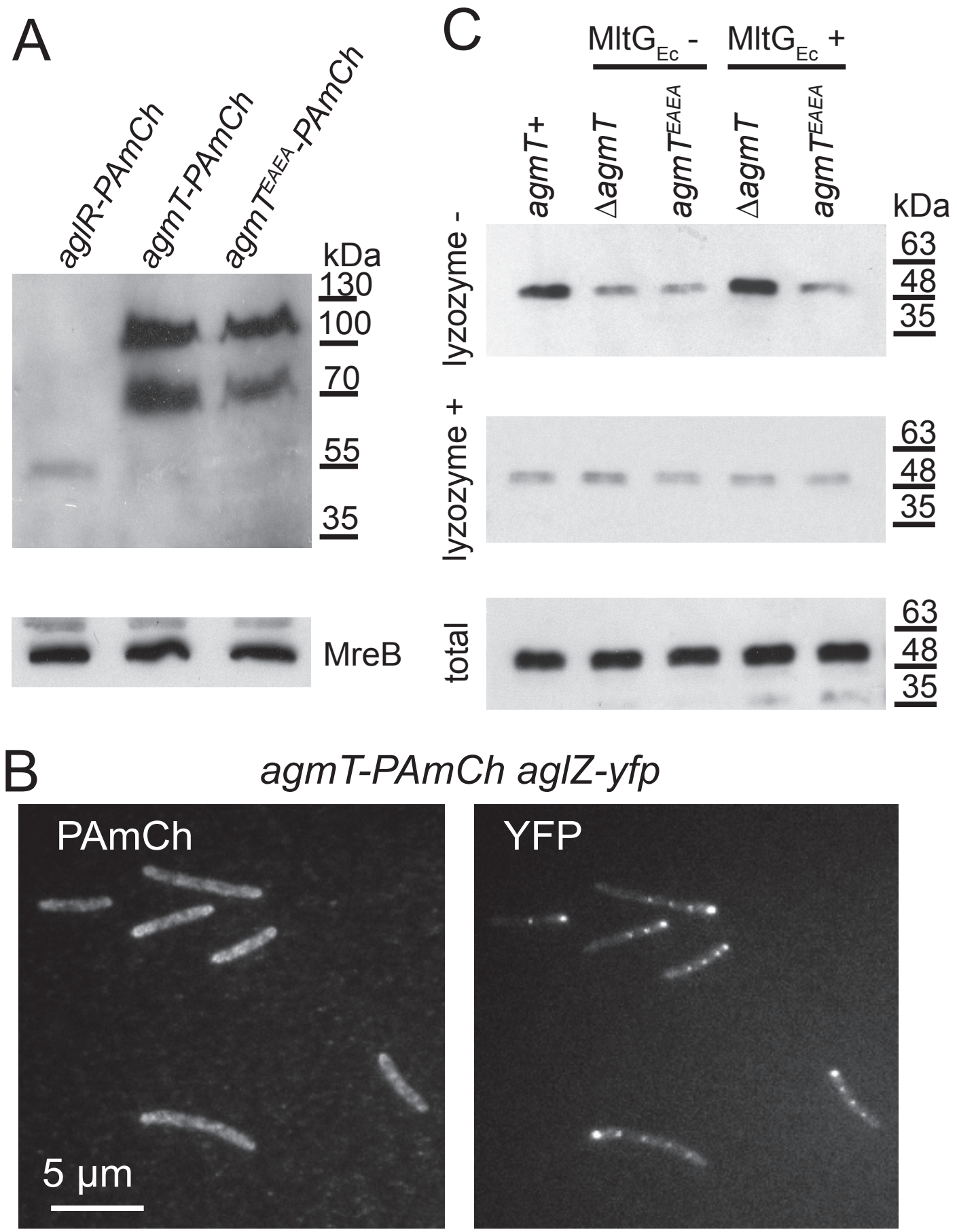
A
aglR-PAmCh
agmT-PAmCh
agmT^EAEA-PAmCh
kDa
130
100
70
55
35
MreB
C
MltG_Ec -
MltG_Ec +
agmT+
ΔagmT
agmT^EAEA
ΔagmT
agmT^EAEA
kDa
lyzozyme -
lyzozyme +
total
63
48
35
B
agmT-PAmCh aglZ-yfp
PAmCh
YFP
5 µm

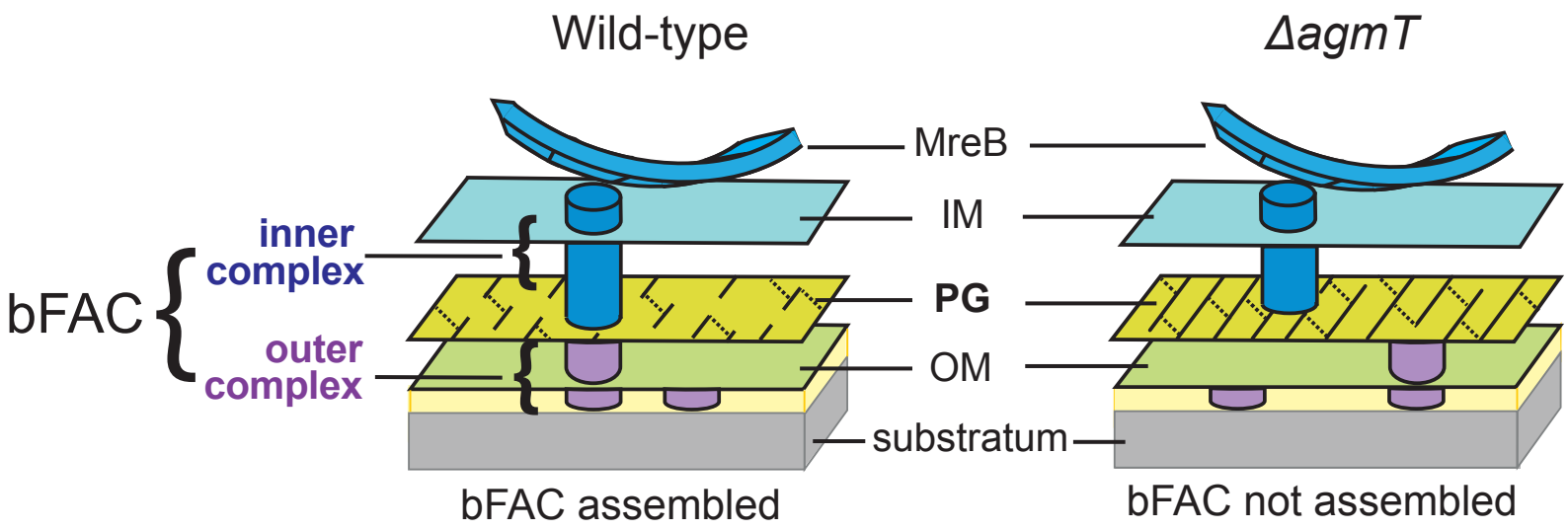
Wild-type
ΔagmT
MreB
IM
PG
OM
substratum
bFAC
inner complex
outer complex
bFAC assembled
bFAC not assembled